JOURNAL OF GUIDANCE, CONTROL, AND DYNAMICS
Vol. 18, No. 5, September–October 1995

Time-Optimal Lateral Maneuvers of an Aircraft

Yigang Fan,* Frederick H. Lutze,† and Eugene M. Cliff‡
Virginia Polytechnic Institute and State University, Blacksburg, Virginia 24061-0203

Results and analysis are presented from a study of time-optimal lateral maneuvers for an aircraft during the power-on-approach-to-landing portion of the flight, typically used for landing on an aircraft carrier. A full six-degree-of-freedom model is used to model the motions of the aircraft. The optimal control problems of interest are formulated and a family of optimal solutions obtained for two classes of lateral maneuvers. These include an unconstrained maneuver and one with bank-angle and sideslip-angle constraints imposed on the approach trajectory. The control powers of elevator, rudder, and aileron are varied individually, and thus an estimate of the change in downrange distance to perform the lateral maneuvers due to the control power change is obtained.

Nomenclature

b	= wing span, ft
C_D	= drag coefficient
C_L	= lift coefficient
C_l	= roll moment coefficient
C_m	= pitch moment coefficient
C_n	= yaw moment coefficient
C_Y	= side force coefficient
c	= mean aerodynamic chord, ft
g	= gravity acceleration, ft/s^2
I_x, I_y, I_z	= principal moments of inertia, slug ft^2
M	= Mach number
m	= mass, slug
p, q, r	= body roll, pitch, and yaw rates, deg/s
S	= reference area, ft^2
T	= engine thrust, lb
T_m	= maximum thrust, lb
v_s	= speed of sound, ft/s
x, y, z	= aircraft position coordinates, ft
α	= angle of attack, deg
β	= sideslip angle, deg
δ_a	= aileron deflection, deg
δ_e	= elevator deflection, deg
δ_r	= rudder deflection, deg
η	= fraction of maximum thrust defined as T/T_m
ρ	= density of air, slug/ft^3
ϕ, θ, ψ	= bank, pitch, and heading angles, deg
χ, γ, μ	= wind axes orientation angles, deg

I. Introduction

SUCCESSFUL landings are generally achieved by ensuring that the speed, glide slope, and runway alignment are within some tolerances during the approach-to-landing portion of the flight. The tolerances allowed are subject to the skills of the pilot, the length and width of the runway, and possibly the wind conditions. These tolerances are probably at their minimum when considering a fighter aircraft approaching a carrier landing. In these cases there are many aids to help the pilot to stay within some specified limits, and if not within these limits, the landing aborted. Although there have been several studies for determining the important factors that influence the probability of having a successful carrier landing,[1] and even more recently, studies have been done that develop automatic controls for carrier landing configuration,[2] there has been little effort to determine optimal maneuvers for recovering from offsets during a carrier landing approach. This paper deals with the optimal lateral maneuver and, to be more specific, the minimum time lateral maneuver. There are several reasons why such a study is of interest. These include establishing a best maneuver against which to judge actual pilot techniques, determining limits on which to base abort requirements, determining how such limits are affected by changing control power about the different axes, and determining how these limits change due to operational constraints such as maximum bank and sideslip.

These maneuvers are generally short and transient in nature, and so the usual methods of optimal trajectory analysis that include reducing the order of the system by assuming point mass models cannot be used if valid results are to be obtained. In addition the maneuvers are short enough that even the control surface rate limits should be considered. Hence the model considered in this study is a full six-degree-of-freedom model with the controls consisting of elevator, rudder, and aileron for moment control and thrust level for longitudinal acceleration control. All of these controls have deflection or magnitude limits in addition to rate limits imposed on them. The aerodynamic models are basically linear with constant coefficients since the speed does not change significantly during the maneuver. In the study, an aerodynamic database for the F/A-18 high angle-of-attack research vehicle (HARV) is used. Accordingly, the numerical results correspond to this aircraft. However, the discussion and methodology presented in the following sections are quite general.

Aircraft maneuvers have been studied by many researchers. But very few of them used the full six-degree-of-freedom model to explore complicated maneuvers for practical aircraft. Bocvarov et al.[3] studied a complicated reorientation maneuver for an aircraft, but they neglected the translational motion of the aircraft and only the rotational motion was analyzed. Dwyer and Lutze[4] are probably the first to use a six-degree-of-freedom model in aircraft maneuver studies and consider the magnitude and rate constraints on the control inputs. But the maneuvers they have explored are not very complicated. So the work presented in this paper is a further development of these previous works.

A mathematical model of the aircraft and the associated aerodynamic forces and moments are presented in Sec. II. The basic ideas and assumptions of the full six-degree-of-freedom model are discussed. In Sec. III, the practical problems of interest for landing on an aircraft carrier are formulated and two classes of lateral maneuvers discussed. In Sec. IV, the optimal control problems of interest are formulated and optimal solutions are obtained by using the graphical environment for solving optimization problems (GESOP) code. In Sec. V, results relating to a family of optimal solutions for two classes of lateral maneuvers during approach configuration are presented. The change in downrange distance to perform the lateral maneuvers, due to the individual variation of the control powers of elevator, rudder, and aileron, is discussed, and numerical results are shown.

Received Dec. 5, 1994; revision received May 16, 1995; accepted for publication May 19, 1995.

*Visiting Scholar, Department of Aerospace and Ocean Engineering.

†Professor, Department of Aerospace and Ocean Engineering. Associate Fellow AIAA.

‡Reynolds Metals Professor, Department of Aerospace and Ocean Engineering. Associate Fellow AIAA.

II. Mathematical Model

The mathematical model of the aircraft, used in the present study, is represented by the following dynamic and kinematic equations[5,6]:

$$\dot{M} = \frac{1}{mv_s}\left[T_m\eta\cos\alpha\cos\beta - C_D\frac{1}{2}\rho(v_sM)^2S - mg\sin\gamma\right]$$

$$\dot{\alpha} = q - \frac{1}{\cos\beta}\left[(p\cos\alpha + r\sin\alpha)\sin\beta + \frac{1}{mv_sM}(T_m\eta\sin\alpha + C_L\frac{1}{2}\rho(v_sM)^2S - mg\cos\mu\cos\gamma)\right]$$

$$\dot{\beta} = \frac{1}{mv_sM}\left[-T_m\eta\cos\alpha\sin\beta + C_Y\frac{1}{2}\rho(v_sM)^2S + mg\sin\mu\cos\gamma\right] + p\sin\alpha - r\cos\alpha$$

$$\begin{aligned}
\dot{p} &= \frac{I_y - I_z}{I_x}qr + \frac{1}{2I_x}\rho(Mv_s)^2SbC_l \\
\dot{q} &= \frac{I_z - I_x}{I_y}pr + \frac{1}{2I_y}\rho(Mv_s)^2ScC_m \\
\dot{r} &= \frac{I_x - I_y}{I_z}pq + \frac{1}{2I_z}\rho(Mv_s)^2SbC_n \\
\dot{\phi} &= p + q\sin\phi\tan\theta + r\cos\phi\tan\theta \\
\dot{\theta} &= q\cos\phi - r\sin\phi \\
\dot{\psi} &= (q\sin\phi + r\cos\phi)\sec\theta \\
\dot{x} &= v_sM\cos\gamma\cos\chi \\
\dot{y} &= v_sM\cos\gamma\sin\chi \\
\dot{z} &= -v_sM\sin\gamma
\end{aligned} \tag{1}$$

Here the body-fixed frame axes are assumed to coincide with the principal axes of inertia of the aircraft.

In Eq. (1), the Mach number is used as a variable since it naturally scales the velocity to be the same order of magnitude as the remaining variables, which is a useful property to take advantage of when solving an optimization problem.

In the right-hand sides of Eqs. (1) appear wind axes orientation variables χ, γ and μ. They are dependent on the state variables ϕ, θ, ψ, α, and β and can be determined using the following equations[6]:

$$\begin{aligned}
\sin\gamma &= \cos\alpha\cos\beta\sin\theta - \sin\beta\sin\phi\cos\theta - \sin\alpha\cos\beta\cos\phi\cos\theta \\
\sin\chi &= \frac{1}{\cos\gamma}[\cos\alpha\cos\beta\cos\theta\sin\psi + \sin\beta(\sin\phi\sin\theta\sin\psi + \cos\phi\cos\psi) + \sin\alpha\cos\beta(\cos\phi\sin\theta\sin\psi - \sin\phi\cos\psi)] \\
\sin\mu &= \frac{1}{\cos\gamma}(\sin\theta\cos\alpha\sin\beta + \sin\phi\cos\theta\cos\beta - \sin\alpha\sin\beta\cos\phi\cos\theta)
\end{aligned} \tag{2}$$

Equations (1), in combination with kinematical relations (2), constitute a full six-degree-of-freedom model of aircraft, used in the present trajectory optimization study.

The coefficients of aerodynamic forces and moments acting on the aircraft are very complex functions, each depending on the angles α and β and body angular rates p, q, and r, as well as the Mach number, altitude, and deflections of all of the aerodynamic control surfaces. However, analyses of aerodynamic data for the HARV show that many of these dependencies can be neglected for the problem considered. For example, because the maneuvers of interest are short, Mach number does not change significantly during the maneuvers. Thus, all of the aerodynamic coefficients can be calculated for a fixed Mach number.

The database for the HARV allows the right and left aerodynamic controls to be operated independently. This capability was not exploited in order to reduce the complexity of this study. In the problems examined here, the left and right elevator and left and right rudder deflections are of equal magnitude and in the same direction. The left and right aileron deflections are of equal magnitude and in opposite directions, with a positive δ_a generating negative roll moment.

The aerodynamic coefficients for the HARV are available in the form of table lookups, the data being given at a certain set of grid points within the intervals $\beta \in (-20\text{ deg}, +20\text{ deg})$ and $\alpha \in (-10\text{ deg}, +90\text{ deg})$. For the present optimization problem of interest, analytical functions for aerodynamic coefficients are developed. All of the six aerodynamic coefficients are represented as analytical functions of α, β, p, q, r, δ_e, δ_a, and δ_r. The functions are generated by using least-square fitting software to match the graphs of the HARV database generated specifically for the aircraft in the landing configuration of interest at $M = 0.2$ and sea level altitude. For these conditions, all of the flaps and ailerons were used, with trailing-edge flaps deflected down 45 deg, leading-edge flaps down 17.6 deg, and both the right and left ailerons down 42 deg. The landing gear is in the down position.

An accurate representation of the aerodynamic coefficients can be obtained if the following functional dependencies are assumed.

1) Drag coefficient:

$$C_D = \begin{cases} 0.0013\alpha^2 - 0.00438\alpha + 0.1423, & -5 \le \alpha \le 20 \\ -0.0000348\alpha^2 + 0.0473\alpha - 0.3580, & 20 \le \alpha \le 40 \end{cases} \tag{3}$$

2) Side force coefficient:

$$C_Y = -0.0186\beta + \frac{\delta_a}{25}(-0.00227\alpha + 0.039) + \frac{\delta_r}{30}(-0.00265\alpha + 0.141) \tag{4}$$

3) Lift coefficient:

$$C_L = \begin{cases} 0.0751\alpha + 0.0144\delta_e + 0.732, & -5 \le \alpha \le 10 \\ -0.00148\alpha^2 + 0.106\alpha + 0.0144\delta_e + 0.569, & 10 \le \alpha \le 40 \end{cases} \tag{5}$$

4) Roll-moment coefficient:

$$C_l = C_l(\alpha, \beta) - 0.0315p + 0.0126r + \frac{\delta_a}{25}(0.00121\alpha - 0.0628) - \frac{\delta_r}{30}(0.000351\alpha - 0.0124) \tag{6}$$

where

$$C_l(\alpha, \beta) = \begin{cases} (-0.00012\alpha - 0.00092)\beta, & -5 \le \alpha \le 15 \\ (0.00022\alpha - 0.006)\beta, & 15 \le \alpha \le 25 \end{cases} \tag{7}$$

5) Pitch-moment coefficient:

$$C_m = -0.00437\alpha - 0.0196\delta_e - 0.123q - 0.1885 \tag{8}$$

6) Yaw-moment coefficient:

$$C_n = C_n(\alpha, \beta) - 0.0142r + \frac{\delta_a}{25}(0.000213\alpha + 0.00128) + \frac{\delta_r}{30}(0.000804\alpha - 0.0474) \tag{9}$$

where

$$C_n(\alpha, \beta) = \begin{cases} 0.00125\beta, & -5 \le \alpha \le 10 \\ (-0.00022\alpha + 0.00342)\beta, & 10 \le \alpha \le 25 \\ -0.00201\beta, & 25 \le \alpha \le 35 \end{cases} \tag{10}$$

In Eqs. (3–10), all angles and control surface deflections are in degrees and angular rates are in radians per second. All functions are continuous.

The basic properties of the HARV for a combat configuration used in present study are

$$\begin{aligned} S &= 400 \text{ ft}^2 & m &= 1036 \text{ slug} \\ b &= 37.42 \text{ ft} & I_x &= 23{,}000 \text{ slug ft}^2 \\ c &= 11.52 \text{ ft} & I_y &= 151{,}293 \text{ slug ft}^2 \\ T_m &= 11{,}200 \text{ lb} & I_z &= 169{,}945 \text{ slug ft}^2 \end{aligned}$$

All of the atmospheric properties (ρ, v_s, ...) are determined at sea level conditions.

III. Problem of Interest

It is generally agreed that a successful landing of an aircraft requires the approach to be stabilized well before touchdown. This requirement is particularly important for landing on an aircraft carrier. Consequently, it is desired to be aligned with the centerline of the landing deck, be at proper approach speed, and be on glide slope at some minimum distance from the touchdown point. Furthermore, one would like to be able to return to these conditions if one is displaced from them. The problem of interest in this paper deals with recovering from a lateral offset position during a power approach to an aircraft carrier landing. Two important aspects of the problem that are of interest are 1) determining the control requirements and subsequent maneuver that would perform this so-called lateral maneuver in an optimal fashion (without pilot technique influencing the results) and 2) determining how changes in control power about the three aircraft axes affect the results.

To be more specific, we would like to determine the maximum lateral offset that can occur at a specified distance from the landing deck and still permit a return to the desired approach conditions for a proper safe landing. Aircraft outside this limit would be "waived off." Equivalently, the problem can be stated as follows: For a given offset condition, minimize the downrange distance required to return to the desired approach conditions, on line, on glide slope, and on speed.

Unfortunately, this particular formulation can lead to unwanted results. For example, the aircraft could essentially reverse its direction and obtain negative downrange distances. To avoid these difficulties, we choose to attack a similar problem: for a given offset condition, find the minimum time to return to the conditions of a desired approach. It will be demonstrated later that the minimum time and the local minimum downrange distance solutions are not exactly the same, but they are sufficiently close for the offset distances included in this paper. Hence, it is practically equivalent to minimize time or downrange distance.

Two classes of such minimum time lateral maneuvers are included in this paper. These are 1) an unconstrained maneuver and 2) a maneuver, with bank-angle and sideslip-angle constraints imposed.

The unconstrained maneuver is of interest so that we can find the largest offset from which the aircraft can return to continue for a successful landing with the available controls. We are also interested in the characteristics of the optimal trajectory and the switching nature of the control histories.

The constrained maneuver is investigated to reflect practical limitations on the power-on-approach-to-landing portion of the flight. During the approach-to-landing phase of flight, large displacements in roll and/or sideslip are not desirable since such maneuvers can easily get out of control or cause vertigo in the pilot. Here we will restrict the bank angle to 30 deg and the sideslip angle to 6 deg to restrict the motions required for recovery from a lateral displacement to what are considered small corrections.

IV. Optimal Control Problem

The mathematical model of the aircraft is represented by Eqs. (1) and (2).

The state variables of the system are given by

$$\boldsymbol{X} = [M, \alpha, \beta, p, q, r, \phi, \theta, \psi, x, y, z]^T \tag{11}$$

The control variables of the system are given by

$$\boldsymbol{u} = [\eta, \delta_e, \delta_r, \delta_a]^T \tag{12}$$

and subject to the following magnitude limits:

$$\begin{aligned} \eta(t) &\in [0.0, +1.0] \\ \delta_e(t) &\in [-24 \text{ deg}, +10.5 \text{ deg}] \\ \delta_r(t) &\in [-30 \text{ deg}, +30 \text{ deg}] \\ \delta_a(t) &\in [-25 \text{ deg}, +25 \text{ deg}] \end{aligned} \tag{13}$$

Note that the aileron deflections are measured relative to the drooped position for landing.

In addition, the controls have the following rate limits:

$$\begin{aligned} |\dot{\eta}(t)| &\le 0.55 \text{ deg/s} \\ |\dot{\delta}_e(t)| &\le 40 \text{ deg/s} \\ |\dot{\delta}_r(t)| &\le 56 \text{ deg/s} \\ |\dot{\delta}_a(t)| &\le 100 \text{ deg/s} \end{aligned} \tag{14}$$

The maneuvers of interest are initiated from steady-state, power-on-approach, symmetric flight with glide slope $\gamma_0 = -3.5$ deg. The initial conditions of the system can be obtained by assuming symmetric steady-state flight and solving the following equations at Mach number = 0.2 for the values of the variables α, δ_e, and η:

$$\begin{aligned} T_m \eta \cos\alpha - C_D \tfrac{1}{2}\rho(v_s M)^2 S - mg \sin\gamma_0 &= 0 \\ T_m \eta \sin\alpha + C_L \tfrac{1}{2}\rho(v_s M)^2 S - mg \cos\gamma_0 &= 0 \\ C_m \tfrac{1}{2}\rho(v_s M)^2 Sc &= 0 \end{aligned} \tag{15}$$

Here, the thrust is assumed to pass through the center of gravity of the aircraft.

The solutions to Eq. (15) are then obtained as $\alpha_0 = 9.96$, $\delta_{e0} = m - 11.86$, and $\eta_0 = 0.254$. Hence the initial values of the state variables are all zero except for

$$\begin{aligned} M(0) &= 0.2 \\ \alpha(0) &= 9.96 \\ \theta(0) &= 6.46 \end{aligned} \tag{16}$$

The initial values of the control variables are

$$\begin{aligned} \boldsymbol{u}(0) &= [\eta(0), \delta_e(0), \delta_r(0), \delta_a(0)]^T \\ &= [0.254, -11.86, 0, 0]^T \end{aligned} \tag{17}$$

During the maneuver, the aircraft transitions from steady-state, power-on-appproach, symmetric flight condition to steady-state, power-on-approach, symmetric flight in the same glide-slope plane shifted laterally by a specified offset distance. Thus, the final conditions for the maneuver can be formulated in the following equality constraint form:

$$\begin{aligned} y(t_f) - y_f &= 0 \\ \gamma(t_f) - \gamma_0 &= 0 \\ x(t_f)\tan\gamma_0 + z(t_f) &= 0 \\ \alpha(t_f) - \alpha_0 &= 0 \\ \beta(t_f) &= 0 \\ \phi(t_f) = 0, \qquad \dot{\alpha}(t_f) &= 0 \\ \psi(t_f) = 0, \qquad \dot{M}(t_f) &= 0 \\ p(t_f) = 0, \qquad \dot{p}(t_f) &= 0 \\ q(t_f) = 0, \qquad \dot{q}(t_f) &= 0 \\ r(t_f) = 0, \qquad \dot{r}(t_f) &= 0 \end{aligned} \tag{18}$$

The performance indices for the minimum time and the minimum downrange distance problems are given by

$$J_t = \int_0^{t_f} 1\,dt = t_f$$
$$J_d = \int_0^{t_f} v_s M \cos\gamma \cos\chi\, dt = x(t_f) \tag{19}$$

The optimal control problem of interest is that for the system (1) and (2), we want to find the controls, satisfying the constraints (13) and (14), to guide the system from the initial conditions (16) and (17) to the final conditions (18) in minimum time. This is the statement for the unconstrained lateral maneuver of interest. For the constrained maneuver, we impose the following additional inequality constraints on the trajectory:

$$|\phi(t)| \leq 30 \text{ deg}$$
$$|\beta(t)| \leq 6 \text{ deg} \tag{20}$$

To obtain solutions to this difficult optimal control problem, we resort to the GESOP code. The code implements the optimization by using either PROMIS or TROPIC, which employ different techniques to transform optimal control problems into finite dimensional nonlinear programming problems (NLP). PROMIS uses multiple shooting with numerical integration, whereas TROPIC uses an integration by direct collocation method. Both allow one to include control rate limits in addition to control magnitude constraints. Details on these methods can be found in Refs. 7–12.

V. Numerical Results

A. Unconstrained Maneuver

Typical minimum time solutions for the two classes of lateral maneuvers of interest are presented. The first type is the unconstrained maneuver that is characterized by the formulation of Eqs. (1), (2), (13), (14), and (16–18) and the first performance index in Eq. (19) with no constraints imposed on the trajectory.

As we mentioned before, we are interested in minimum downrange distance solution, and so for the offset condition $y_f = 100$ ft, we solved both the minimum time and the minimum distance problems and found 1) the trajectory and switching nature of aerodynamic controls are almost the same and 2) differences of the thrust histories exist between these two optimal control problems.

Figure 1 shows the engine thrust histories for the minimum time and the minimum distance problems. The solid line in Fig. 1 represents the thrust history $\eta_t(t)$ of the time-optimal problem. As one can see, the switching nature of the thrust rate is "Bang-Bang." At the beginning, the aircraft increases the thrust at the maximum rate, keeping the speed as high as possible, then reduces the thrust at maximum rate, making the speed satisfy the final conditions. The dashed line represents the thrust history $\eta_d(t)$ of the minimum downrange solution. There is a tradeoff, actually, in one aspect; the aircraft tries to reduce the speed to minimize the distance. On the other hand, the aircraft wants to increase the speed, making the system respond to controls fast, resulting in a short downrange distance. As a result of the initial reduction in engine thrust, the aircraft tends to drop below the glide slope more than for the minimum time problem. Consequently, it was felt that minimum distance solutions were less safe than the minimum time solutions.

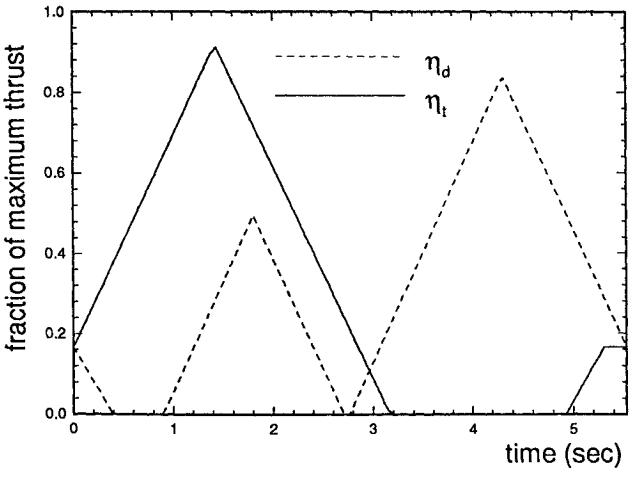

Fig. 1 Fraction of maximum thrust vs time.

The time to do the minimum downrange maneuver is 0.2 s longer but the corresponding downrange distance is 23.8 ft shorter than those of minimum time maneuver. From the figure, one can see a 0.2-s flat region at equilibrium value of the thrust history of the minimum time maneuver. This is because this maneuver is 0.2 s shorter.

Generally speaking, these two maneuvers are not exactly the same, but the results are very close. So we can deal with the minimum time problem instead of the one of minimum downrange distance for the offset conditions included in this paper.

Details about the time-optimal trajectory with an offset condition $y_f = 100$ ft are shown in Figs. 2a–2f. Since the Mach number does not change significantly during the maneuver, the associated trajectory is nearly a straight line and is not plotted.

The roll motion of the aircraft is shown in Fig. 2a, and the angle of attack and sideslip information is shown in Fig. 2b. As expected, the vehicle rolls to initiate the lateral maneuver and at the same time increases angle of attack to increase the lift. At peak angle of attack, the roll is reversed as quickly as possible to take out the side velocity after which the aircraft rolls to a wings-level attitude and reduces its angle of attack to the steady-state value. In addition, from Fig. 2a we can observe the extremes of the motion. The vehicle bank angle ϕ and the velocity bank angle μ are almost coincident. The ranges of these two angles are $|\phi(t)| \leq 70.0$ deg and $|\mu(t)| \leq 67.4$ deg. The roll rate history is also shown in Fig. 2a with extreme values whose magnitude is 115 deg/s, with rapid reversals.

In addition to angle of attack, Fig. 2b shows the sideslip angle β and the vehicle pitch angle θ. The sideslip angle reaches the extreme value of 15 deg, switching rapidly from positive to negative values as the aircraft goes through its rapid roll reversal. It appears that these large sideslip angles are developed due to the aircraft tendency to roll around its body axis as opposed to about the velocity vector. Hence a rapid positive roll would tend to produce a positive sideslip. This same idea explains the nonuniform increase (and decrease) in angle of attack observed in Fig. 2b.

Figure 2c shows the yaw motion of the aircraft along with the flight-path angle. Of particular interest here is a comparison of the velocity yaw and body yaw angles. The velocity yaw angle χ starts out and ends at zero, with the velocity pointing in the desired direction. During the lateral maneuver, it builds to a maximum value of 12.4 deg and then returns smoothly to zero. The shape of the curve is very nearly symmetric with the time of the maneuver; i.e., the peak occurs at the midpoint. The vehicle yaw angle appears to lead the velocity yaw angle during the first portion of the maneuver and then appears to overshoot during the final portion of the maneuver. This phenomenon occurs due to the combination of the roll angle and the angle of attack. A vehicle with zero sideslip and rolled 90 deg would have a vehicle yaw angle equal to the velocity yaw angle plus the angle of attack. The apparent overshoot occurs for the same reason. The angle of attack causes the vehicle axis to point beyond the desired direction before the aircraft rolls to level.

Figure 2d shows the aircraft pitch and yaw rate histories. Of particular interest here is the pitch rate activity with extremes at ± 17 deg/s, with the rapid reversal between 2 and 3 s into the maneuver.

Figure 2e shows the recovery of the offset distance and the change of altitude as the time histories (y_l, z_l). The x coordinate is not shown here because it is virtually linear with time. If we look at the flight-path angle curve in Fig. 2c and the altitude curve in Fig. 2e, we can see that the aircraft drops slightly below the glide slope-plane during the maneuver, probably not a desirable feature. It turns out that for shorter lateral distances the aircraft actually moves above the glide-slope as it does initially here. For the offset condition $y_f = 100$ ft, the downrange distance is 1246.5 ft. The Mach number keeps nearly constant during the maneuver. The minimum time to accomplish the maneuver is 5.3 s.

Figure 2f shows the aerodynamic control histories that generate the mentioned roll, pitch, and yaw motions. It can be observed that all

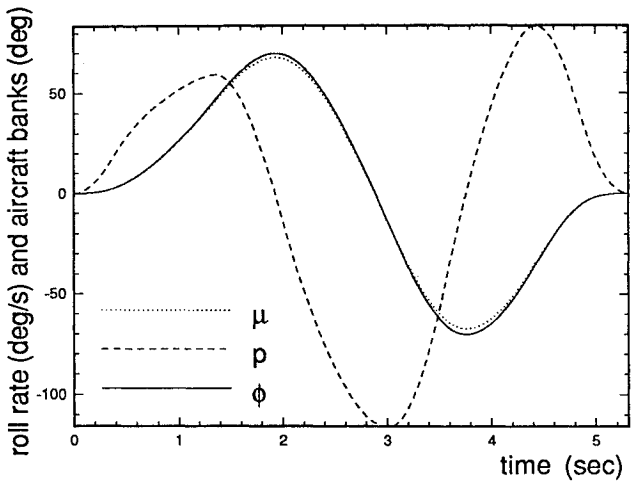

Fig. 2a Angles ϕ and μ and roll rate p vs time.

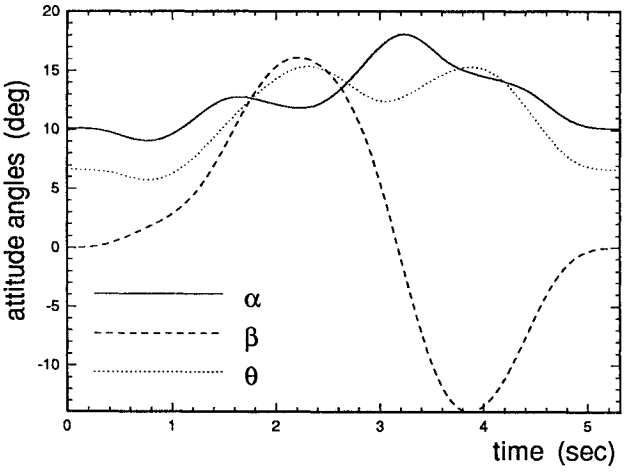

Fig. 2b Angles α and β and θ vs time.

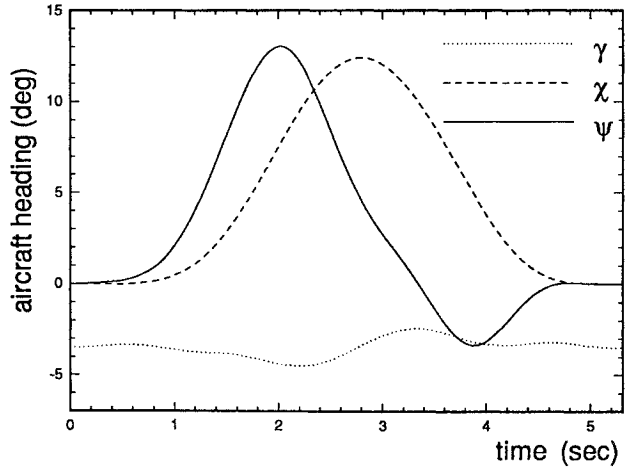

Fig. 2c Angles γ and χ and ψ vs time.

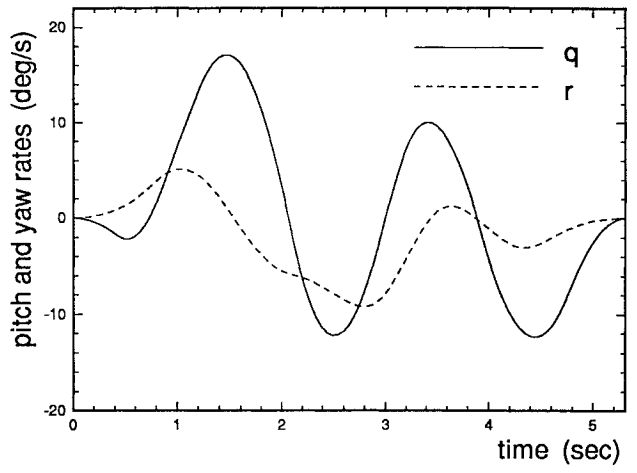

Fig. 2d Pitch and yaw rates q and r vs time.

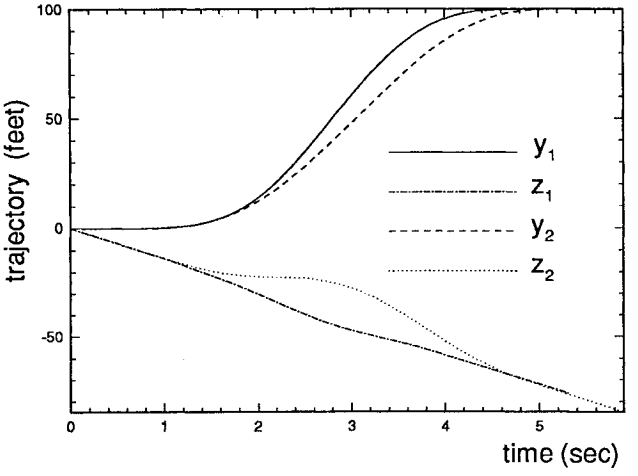

Fig. 2e Trajectory coordinates y and z vs time.

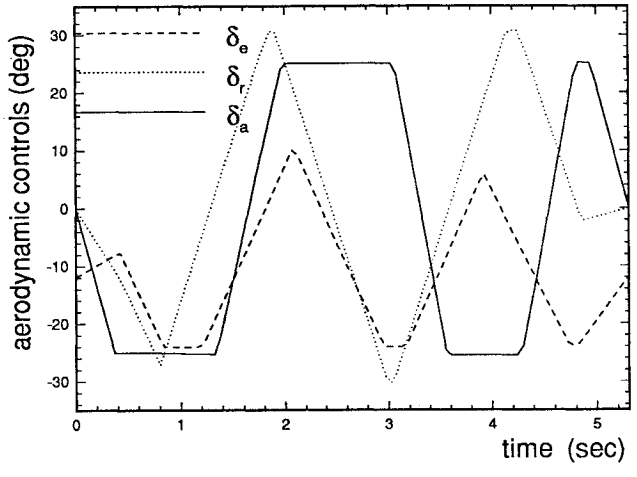

Fig. 2f Aerodynamic controls vs time.

controls reach their limits at one time or another. Also in almost all cases the controls are moving at their rate limits. The ailerons are always at their rate or physical limits. Furthermore, the aileron behavior shows three switches (sign changes) during the maneuver. The elevator shows short non-rate-limited behavior at both the beginning and end of the maneuver. Otherwise all motion is rate limited or at the physical limits. One can notice that the second peak in the elevator deflection curve is not at its limit but is the intersection of two rate-limited segments. Finally with regard to the elevator one can note the rapid down-up-down elevator command that occurs between 1 and 5 s into the maneuver. One would not expect a pilot to provide this kind of input during a carrier approach, but it is optimal.

B. Constrained Maneuver

The second type of lateral maneuver of interest is the constrained one. In addition to the formulation of the unconstrained maneuver, we impose additional constraints (20) on the trajectory. Details of the solutions for the constrained optimal trajectory with the same offset condition $y_f = 100$ ft are shown in Figs. 3a–3e.

Figure 3a shows the roll motion of aircraft during the maneuver. The basic properties are the same as those in Fig. 2a, but the bank angle ϕ and velocity bank μ are confined to the range ± 30 deg, whereas those of unconstrained maneuver are approximately two times bigger.

Pitch motion of aircraft is shown in Fig. 3b from which one can see that a slight difference exists from the unconstrained maneuver.

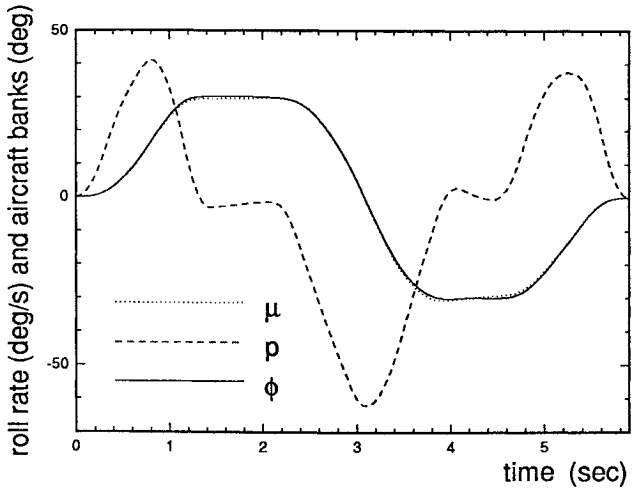

Fig. 3a Angles ϕ and μ and roll rate p vs time.

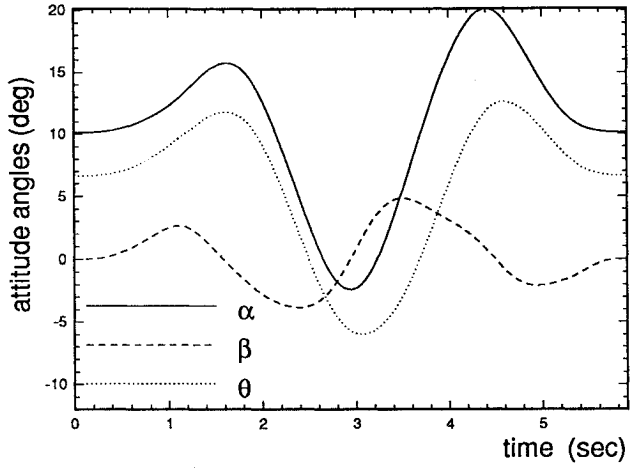

Fig. 3b Angles α and β and θ vs time.

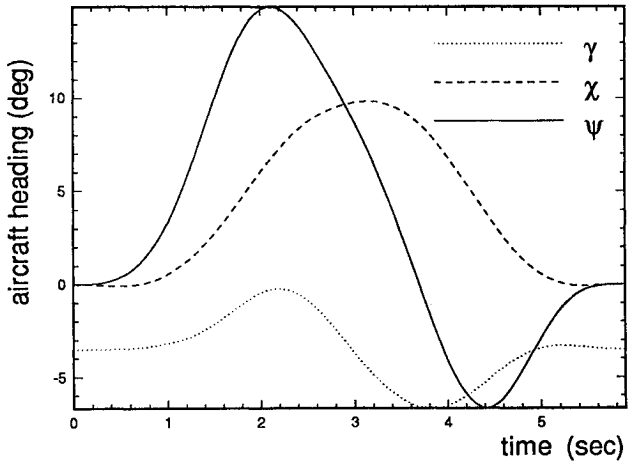

Fig. 3c Angles γ and χ and ψ vs time.

The aircraft pitches up, while rolling to the positive limit, obtaining more lift to recover the offset distance, then pitches down, while rolling back, and then pitches up again, while rolling to the negative limit, obtaining more lift to slow down the ongoing offset movement. The angle of attack reaches the extreme value of 20 deg. The pitch rate is shown in Fig. 3d with the extreme values whose magnitude is 22 deg/s, with rapid reversals. One can notice that the extremes of pitch rate and angle of attack are bigger than those of the unconstrained maneuver (Figs. 2b and 2d). The reason for this is that since the constraints on bank and sideslip are imposed on the trajectory, the aircraft needs to make better use of unconstrained pitch motion to perform the lateral maneuver. With bigger pitch rate and then the

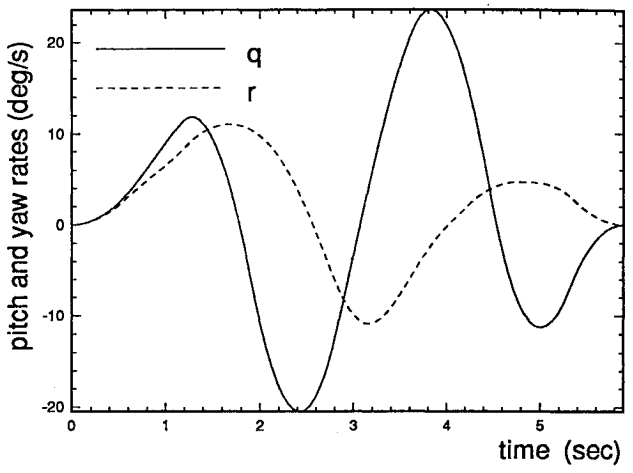

Fig. 3d Pitch and yaw rates q and r vs time.

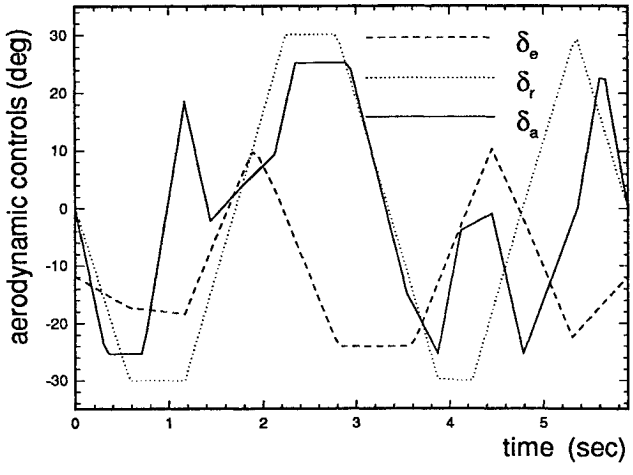

Fig. 3e Aerodynamic controls vs time.

bigger angle of attack, the aircraft obtains more lift that can be used to recover the offset distance even with limited roll motion.

The properties of yaw motion shown in Fig. 3c are similar to those of the unconstrained maneuver. The corresponding yaw rate is shown in Fig. 3d. The offset distance recovery and the change of altitude are shown with those of the unconstrained maneuver in Fig. 2e as the time histories (y_2, z_2). From the figure, one can see that, different from the unconstrained maneuver, the aircraft goes up slightly above the glide-slope plane during the maneuver. This is because of the relatively bigger pitch rate and angle of attack in performing this lateral maneuver. The downrange distance of the maneuver is 1386.8 ft, which is 140.3 ft longer than that of the unconstrained maneuver. The minimum time to accomplish the maneuver is 5.9 s, compared with 5.3 s for the unconstrained maneuver.

Figure 3e shows the aerodynamic control histories that generate the roll, pitch, and yaw motions. Nothing is new to the switching nature of elevator and rudder histories. For the roll channel, since the bank angle is limited to ± 30 deg, it is not necessary to deflect the aileron to maximum magnitude all of the time. Thrust control is of the same configuration as that of unconstrained maneuver.

To determine the lateral offset limit that can occur at a specified distance from the landing deck and still permit a return to the desired approach conditions for a proper safe landing, we solved a series of unconstrained and constrained optimal control problems for several specified offset conditions and obtained the corresponding downrange distances that are needed for a recovery in minimum time. Figure 4 shows these limits. Aircraft inside these limits will be able to recover from a lateral offset position and continue to the desired approach conditions for a successful landing.

We are interested in determining how changes in the control power of each aerodynamic surface affect the results. The control power here is defined as the moment generated per unit control surface deflection about that axis. To answer this question, we change the

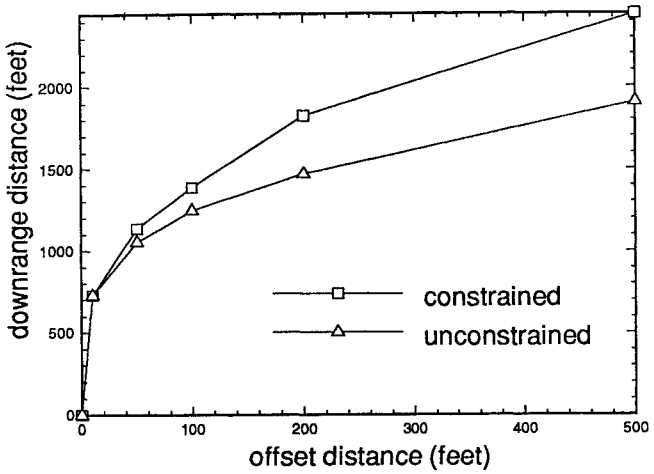

Fig. 4 Limits to recover from a lateral offset position.

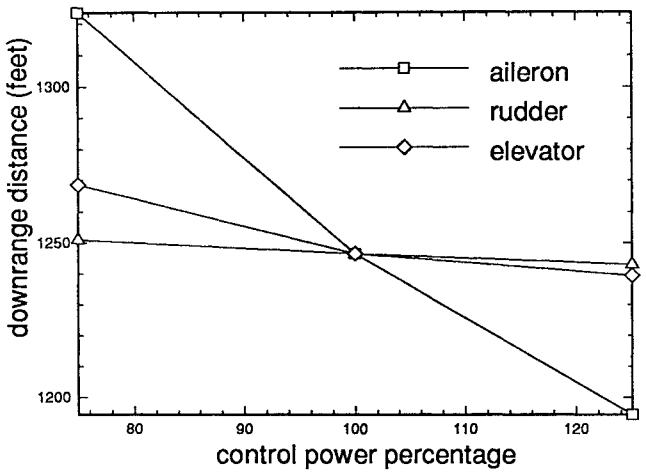

Fig. 5 Effects of control powers (unconstrained).

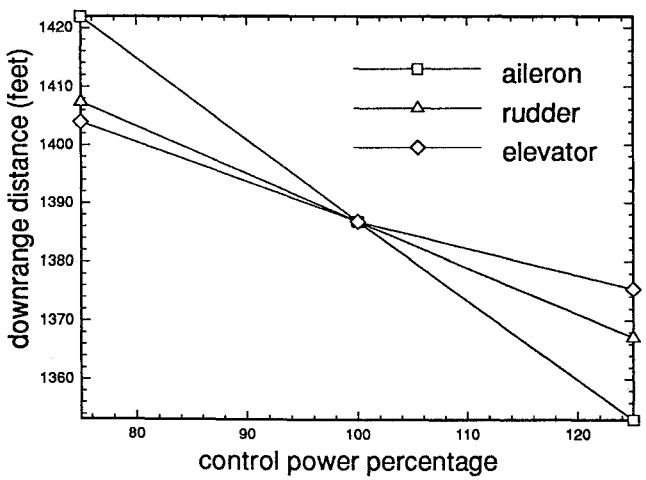

Fig. 6 Effects of control powers (constrained).

control powers of elevator, rudder, and aileron individually, by 25%, and solve the corresponding optimal control problems for the lateral offset condition $y_f = 100$ ft. The results are shown in Fig. 5 for unconstrained maneuvers and in Fig. 6 for constrained maneuvers.

From Fig. 5, one can see, for unconstrained maneuvers, that the downrange distances needed to recover from the specified offset position are not linear with the changes of control power for each of the aerodynamic surfaces. Since no constraint is imposed on the bank, full use of the aileron is made in performing the maneuvers. As expected, the changes of the control power of the aileron affect the results significantly. Compared with the aileron, the effects of the control powers of the elevator and the rudder are small. More specifically, changing control power by 25%, the change of downrange distance is approximately 65 ft for the aileron, 12 ft for the elevator, and only 4 ft for the rudder.

The results for constrained maneuvers are shown in Fig. 6 from which one can see that the downrange distances needed to perform the maneuvers are almost linear with the changes of control power for all of the aerodynamic surfaces. The control power of the aileron still affects the results the most but not as significantly because the constraints on the bank and the sideslip are imposed on the trajectory. The rudder and the elevator become more important in constrained maneuvers but reverse their importance from unconstrained maneuvers, the effect of the control power of the rudder coming second instead of last. Numerically, increasing control power by 25%, the downrange distance is reduced by 33.7 ft for the aileron, by 19.7 ft for the rudder, and by 11.5 ft for the elevator.

We also studied the control power effects for different offset conditions. The results show that the changes of downrange distance due to the changes of the control powers are almost the same at different offset conditions.

VI. Conclusions

Based on a full six-degree-of-freedom model, two classes of lateral maneuvers for an aircraft during power-on-approach-to-landing portion of flight have been studied. The lateral offset limits of interest, which can occur at a specified distance from the landing deck and still permit a return to the desired approach conditions for a proper safe landing, have been numerically determined for unconstrained and constrained maneuvers. The effects of the control powers of aileron, rudder, and elevator on the downrange distance for some specified offset conditions have been studied individually. Corresponding results are shown. This work also shows that it is possible to use the GESOP code, combined with certain engineering techniques, to analyze and solve optimal control problems for highly complex dynamic systems.

Acknowledgments

This research was supported in part by the NASA Langley Research Center, Grant NCC1-158-2 and Grant NAG-1-1405, and in part by the Naval Air Warfare Center, Contract N60921-89D-A239-0031.

References

[1]Durand, T. S., and Wasicko, R. J., "Factors Influencing Glide Path Control in Carrier Landing," *Journal of Aircraft*, Vol. 4, No. 2, 1967, pp. 146–158.

[2]Urnes, J. M., and Hess, R. K., "Development of the F/A-18A Automatic Carrier Landing System," *Journal of Guidance, Control, and Dynamics*, Vol. 8, No. 3, 1985, pp. 289–295.

[3]Bocvarov, S., Lutze, F. H., and Cliff, E. M., "Time-Optimal Reorientation Maneuvers for a Combat Aircraft," *Journal of Guidance, Control, and Dynamics*, Vol. 16, No. 2, 1993, pp. 232–240.

[4]Dwyer, M. E., and Lutze, F. H., "Quasi-Optimal Steady State and Transient Maneuvers with and without Thrust Vectoring," AIAA Paper 93-3778, Aug. 1993.

[5]Etkin, B., *Dynamics of Atmospheric Flight*, Wiley, New York, 1972.

[6]Fan, Y., Lutze, F. H., and Cliff, E. M., "Time-Optimal Sidestep Maneuvers of Aircraft," AIAA Paper 94-3495, Aug. 1994.

[7]Well, K. H., and Ebert, K., "Trajectory Optimization Techniques and Software Implementation," IFAC Symposium on Aerospace Control, Ottobran, Sept. 1992.

[8]Dickmanns, E. D., and Well, K. H., "Approximate Solution of Optimal Control Problems Using Third-Order Hermite Polynominal Functions," *Proceedings of the 6th Technical Conference on Optimization Techniques*, IFIP-TC7, Springer–Verlag, New York, 1975.

[9]Hargraves, C. R., and Paris, S. W., "Direct Trajectory Optimization Using Nonlinear Programming and Collocation," *Journal of Guidance, Control, and Dynamics*, Vol. 10, No. 4, 1987, pp. 338–342.

[10]Kraft, D., "On Converting Optimal Control Problems into Nonlinear Programming Problems," NATO ASI Series, Vol. F 15, Computational Mathematical Programming, Springer–Verlag, 1985.

[11]Rader, J. E., and Hull, D. G., "Computation of Optimal Aircraft Trajectories Using Parameter Optimization Methods," *Journal of Aircraft*, Vol. 12, Nov. 1975, pp. 864–866.

[12]Hargraves, C. R., Johnson, F. T., Paris, S. W., and Rettie, I., "Numerical Computation of Optimal Atmospheric Trajectories," *Journal of Guidance and Control*, Vol. 4, No. 4, 1981, pp. 406–414.